Composite finite volume schemes for the diffusion equation on unstructured meshes

Xavier Blanc, Philippe Hoch, Clément Lasuen

Composite finite volume schemes for the diffusion equation on unstructured meshes

Xavier Blanc[1], Philippe Hoch[2], Clément Lasuen[2]

[1]Université Paris Cité, CNRS, Sorbonne Université,
Laboratoire Jacques-Louis Lions (LJLL), F-75006 Paris,
xavier.blanc@u-paris.fr

[2]CEA, DAM, DIF, F-91297 Arpajon, France
philippe.hoch@cea.fr clement.lasuen@cea.fr

October 13, 2023

Abstract

We present a finite volume scheme for the anisotropic diffusion equation. The scheme is based on a reformulation of the diffusion equation as an advection equation. We prove that it is first order consistent and stable under a parabolic CFL condition. We propose a second order extension with similar properties. We also propose a third order extension. Numerical tests are provided, confirming the expected properties of the scheme.

Contents

1 Introduction

In this work, we study a finite volume scheme for the anisotropic diffusion equation (1) in two space dimensions:

$$\partial_t E - \text{div } (\kappa \nabla E) = \mathcal{S}. \tag{1}$$

For simplicity, we assume that periodic boundary conditions are imposed. However, what follows may be adapted to more general boundary conditions, such as Dirichlet, Neumann, or mixed boundary conditions. The unknown is denoted by E. The diffusion tensor is κ and we assume that, for any $\mathbf{x} \in \Omega$ (Ω being the domain of computation), $\kappa(\mathbf{x})$ is a symmetric positive definite 2×2 matrix. The source term $\mathcal{S}$ is non-negative and depends on time and space. We also assume that there exists $\kappa_2 \geq \kappa_1 > 0$ such that:

$$\forall \mathbf{x} \in \Omega,\ \text{Sp}(\kappa(\mathbf{x})) \subset [\kappa_1, \kappa_2]. \tag{2}$$

Under Assumptions (2), Equation (1) is well-posed (see [RB17] for instance). Moreover, if the initial data and the source term are positive, then we have:

$$\forall t \geq 0, \quad \forall \mathbf{x} \in \Omega, \quad E(t, \mathbf{x}) > 0. \tag{3}$$

Another important property is that Equation (1) is conservative, that is, any solution satisfies the following equality:

$$\frac{d}{dt} \int_\Omega E(t, \mathbf{x}) d\mathbf{x} = \int_\Omega \mathcal{S}(\mathbf{x}) d\mathbf{x}. \tag{4}$$

In the present work, we propose a finite volume scheme for (1) that is based on a reformulation of Equation (1) as a transport equation:

$$\partial_t E + \text{div } (E \kappa \mathbf{u}) = \mathcal{S}, \qquad \mathbf{u} = -\frac{\nabla E}{E}. \tag{5}$$

Owing to (3), Equation (5) is well defined. In [Fra12] and [FBD11], a finite volume scheme was proposed for equation (1) using the formulation (5). Such a scheme uses nodal fluxes. In [BHL21], this scheme was generalized to conical meshes (that is, meshes the edges of which are defined by conical curves), using ideas from [Hoc22]. The use of conical meshes naturally induces additionnal edge fluxes. This has the advantage of improving stability, while keeping the same convergence rate. This holds even if the conical mesh scheme is restricted to polygonal meshes. Doing so, we obtain what we call a composite scheme that combines both nodal and edge fluxes. In the present work, we concentrate on this composite scheme on polygonal meshes.

The question of defining an accurate finite volume scheme for the diffusion equation on deformed meshes is a long-standing problem. It is well-known that a standard two-point flux is consistent only on rectangular meshes. To our knowledge, the first attempt to design a consistent scheme is that of D. Kershaw [Ker81]. This scheme was not proved to be consistent on general meshes, and numerical tests indicate that it is convergent only when cells are parallelograms. This scheme does not satisfy the maximum principle, and an attempt to make it positive was proposed in [Per81]. Apart from this scheme, the diamond scheme was analyzed in [CVV99], and proved to be consistent. In such a strategy, one uses node values as auxiliary unknowns, allowing to compute consistent fluxes. These auxiliary unknowns are computed using interpolation. It is also possible to use a mixed finite element approach [RT83] and recast it as a finite volume method (see [AWY97]). Such a scheme is consistent, but not positive. Another approach, called DDFV (Discrete Duality Finite Volume) was proposed by F. Hermeline in [Her98, Her00, Her03, Her07]. In this strategy, instead of computing the auxiliary (nodal) unknowns by interpolation, they are defined as a solution to a diffusion problem on a dual mesh. Several other methods were proposed, such as the mimetic finite difference method (see, for instance, [BBL09, LMS14]), or the SUSHI (Scheme Using Stabilization and Harmonic Interfaces) method, by R. Eymard, T. Gallouët and R. Herbin [Eym10]. Let us also mention the MPFA (Multi Point Flux Approximation) method proposed in [AEK$^+$07, BM07].

All the above schemes are convergent, but are not positive, in the sense that property (3) is not reproduced at the discrete level. This may be an important issue in applications, since the unknown may be a temperature

or a concentration. A truncation strategy is in principle possible. However, the conservation property (4) is lost in such a process. Note that conservation is also important in applications we have in mind, because Equation (1) should be seen as an elementary building block of a larger system of hyperbolic nature (think of fluid dynamics for instance), for which conservation allows to recover correct shock velocities.
To address the problem of positivity, several strategies have been proposed. Most of them consist in using different consistent estimations of the fluxes and in combining them so that the matrix of the scheme becomes an M-matrix, thereby recovering positivity. Such a strategy was initially proposed in [BM05] and [LP09]. It makes the scheme nonlinear, even though the considered equation (1) is linear. Following these works, many similar strategies have been proposed. Let us cite [LMS14, YSGN22, SY16, SYY09, AN21, WPL$^+$22, NSL22, BL16], among others. Of course, we do not claim this list to be exhaustive.

In the present work, we propose a family of schemes that are naturally consistent, conservative and positive. In contrast with the above mentioned works, positivity is not enforced by modifying an existing non-positive scheme. The starting point of our approach are schemes defined in [FBD11, BHL21] for the M1 model [DF99], which is a hyperbolic nonlinear model that satisfies a positivity principle and a diffusion limit. Since the scheme proposed in [FBD11, BHL21] is asymptotic preserving, it gives a diffusion scheme in this limit. The positivity principle passes to the limit, so this diffusion scheme is positive. It is however only first-order consistent. We therefore propose a second-order extension using gradient reconstruction and second-order quadrature rules for the fluxes. A third-order extension is also proposed and tested.

The present article is organised as follows. In Section 2 we define the notations and give some important geometrical properties. We present the finite-volume scheme that we use to discretise Equation (5) in Section (3). Our scheme uses approximations of E and of $\mathbf{u}$ at the nodes and the midpoints of the edges of the cells. Their computations is described in the subsequent Sections: in Section 4 the first-order scheme, which is based on an upwind strategy. In Section 5 the second-order extension, and in Section 6 the third-order extension. Some numerical examples are presented in Section 7.

2 Notations and geometrical assumptions

In order to make the algebra clearer, vectors are denoted in **bold** in the rest of the paper.

2.1 Composite normal vectors set on unstructured meshes and properties

We present here some notations that will be used in the remainder of the paper. Let Ω_j be a cell of the mesh $\mathcal{T}$ paving the domain Ω. Let $\mathbf{x}_{r-1}$, $\mathbf{x}_r$ and $\mathbf{x}_{r+1}$ be 3 consecutive nodes of Ω_j. We define:

- $(\mathbf{x}_r)_r$ the coordinates of the vertices of the cell j;
- the middle of the edge $[\mathbf{x}_r, \mathbf{x}_{r+1}]$: $\mathbf{x}_{r+1/2} = (\mathbf{x}_r + \mathbf{x}_{r+1})/2$,
- the normal to the edge $[\mathbf{x}_r, \mathbf{x}_{r+1}]$: $\mathbf{C}_j^{r+1/2} = (\mathbf{x}_{r+1} - \mathbf{x}_r)^\perp$,
- the normal to the node r:

$$\mathbf{C}_j^r = \frac{1}{2}(\mathbf{x}_{r+1} - \mathbf{x}_{r-1})^\perp = \frac{1}{2}\left(\mathbf{C}_j^{r+1/2} + \mathbf{C}_j^{r-1/2}\right), \tag{6}$$

where, for any vector $\boldsymbol{\xi} \in \mathbb{R}^2$:

$$\boldsymbol{\xi} = \begin{pmatrix}\xi_1\\ \xi_2\end{pmatrix}, \qquad \boldsymbol{\xi}^\perp = \begin{pmatrix}-\xi_2\\ \xi_1\end{pmatrix}.$$

We define a *degree of freedom* (*dof*) as either a node or a middle of an edge. We also define:

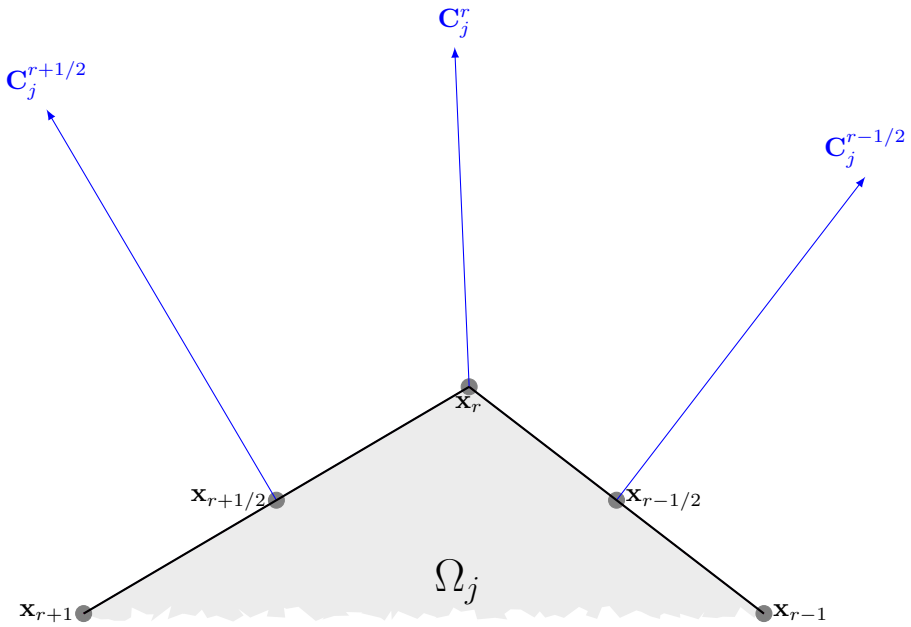

Figure 1: Normals at nodes, at edges : composite set

- $\sum_{r\in\Omega_j} g_j^r$ the sum over all the vertices of the cell j of the quantity g (g_j^r being the evaluation of the function g on the vertex r in cell j);
- $\sum_{r+1/2\in\Omega_j} g_j^{r+1/2}$ the sum over all the mid-edge points of the cell j of the quantity g;
- $N_{\text{dof}} = \sum_{i|\text{dof}\in\Omega_i} 1$ the number of cells that contains the given degree of freedom dof;
- $\sum_{i|\text{dof}\in\Omega_i} g_i^{\text{dof}}$ the sum, for a given degree of freedom, over all the cells that contains this degree of freedom;
- $\sum_{j\in\mathcal{T}} g_j$ the sum over all the cells of the mesh;
- $\sum_{r\in\mathcal{T}} g^r$ the sum over all the nodes of the mesh;
- $\sum_{r+1/2\in\mathcal{T}} g^{r+1/2}$ the sum over all the mid-edge points of the mesh;
- h the maximum length of edges of the mesh,
- $\langle\cdot,\cdot\rangle$ the inner product in $\mathbb{R}^2$.

We have the following quadrature formula.

Theorem 2.1. *Let $g \in \mathcal{C}^2(\mathbb{R}^2;\mathbb{R})$. Then, for all $\theta \in [0,1]$:*

$$\frac{1}{|\Omega_j|}\int_{\partial\Omega_j} g\mathbf{n} = \frac{1}{|\Omega_j|}\left[(1-\theta)\sum_{r\in\Omega_j} g(\mathbf{x}_r)\mathbf{C}_j^r + \theta \sum_{r+1/2\in\Omega_j} g(\mathbf{x}_{r+1/2})\mathbf{C}_j^{r+1/2}\right] + \mathcal{O}(h). \tag{7}$$

Moreover, the remainder in (7) vanishes if g is an affine function.

Moreover, if the parameter θ is set to $2/3$, we have a better result:

Theorem 2.2. *Let $g \in \mathcal{C}^2(\mathbb{R}^2;\mathbb{R})$. Then:*

$$\frac{1}{|\Omega_j|}\int_{\partial\Omega_j} g\mathbf{n} = \frac{1}{|\Omega_j|}\left[\frac{1}{3}\sum_{r\in\Omega_j} g(\mathbf{x}_r)\mathbf{C}_j^r + \frac{2}{3}\sum_{r+1/2\in\Omega_j} g(\mathbf{x}_{r+1/2})\mathbf{C}_j^{r+1/2}\right] + \mathcal{O}(h^2). \tag{8}$$

Moreover, the remainder in (8) vanishes if g is an affine or quadratic function.

The following result is useful in the rest of the paper.

Proposition 2.3. *For any inner node r and any inner edge $r+1/2$:*

$$\sum_{i|r\in\Omega_i} \mathbf{C}_i^r = \sum_{i|r+1/2\in\Omega_i} \mathbf{C}_i^{r+1/2} = \mathbf{0}.$$

2.2 Assumptions on the mesh

We present here the assumptions on the regularity of the mesh. We denote by h the maximal length of the edges of the mesh ($h = \Delta x$ for a cartesian mesh). We assume that there exists a constant C_1 such that, for any dof and any cell j:

$$\frac{1}{C_1}h^2 \le |\Omega_j| \le C_1 h^2, \qquad \|\mathbf{C}_j^{\mathrm{dof}}\| \le C_1 h, \qquad N_{\mathrm{dof}} \le C_1, \tag{9}$$

$$\forall \boldsymbol{\xi} \in \mathbb{R}^2,\ \langle \beta_r \boldsymbol{\xi}, \boldsymbol{\xi}\rangle \ge \frac{1}{C_1}h^2\|\boldsymbol{\xi}\|^2, \tag{10}$$

and thus β_r is non-singular and we have:

$$\|\beta_r^{-1}\| \le C_1 \frac{1}{h^2}. \tag{11}$$

Assumption (10) is studied in [Fra12].

3 Finite volume formulation for the diffusion equation

Integrating Equation (5) leads to:

$$|\Omega_j|\frac{d}{dt}E_j + \int_{\partial\Omega_j}\langle \kappa\nabla E, \mathbf{n}\rangle = |\Omega_j|\mathcal{S}_j, \tag{12}$$

where E_j and $\mathcal{S}_j$ are the mean values of E and $\mathcal{S}$ on the cell Ω_j and $\mathbf{n}$ is the unit outward vector to $\partial\Omega_j$. Using Theorem 2.1, the flux in Equation (12) is approximated by;

$$\int_{\partial\Omega_j}\langle \kappa\nabla E, \mathbf{n}\rangle \approx (1-\theta)\sum_{r\in\Omega_j}\left\langle \kappa_r\mathbf{u}_r, \mathbf{C}_j^r\right\rangle E_j^r + \theta\sum_{r+1/2\in\Omega_j}\left\langle \kappa_{r+1/2}\mathbf{u}_{r+1/2}, \mathbf{C}_j^{r+1/2}\right\rangle E_j^{r+1/2},$$

The vector $\mathbf{u}_{\mathrm{dof}}$ is an approximation of $-\nabla E/E$ at point $\mathbf{x}_{\mathrm{dof}}$ and E_j^{dof} is an approximation of E at point $\mathbf{x}_{\mathrm{dof}}$ in cell j. The latter is computed using an upwind scheme:

$$E_j^{\mathrm{dof}} = \begin{cases} \bar{E}_j^{\mathrm{dof}} & \text{if } \langle \kappa_{\mathrm{dof}}\mathbf{u}_{\mathrm{dof}}, \mathbf{C}_j^{\mathrm{dof}}\rangle > 0, \\ \dfrac{1}{\sum_{i\in I_{\mathrm{dof}}^+}\langle \kappa_{\mathrm{dof}}\mathbf{u}_{\mathrm{dof}}, \mathbf{C}_i^{\mathrm{dof}}\rangle}\displaystyle\sum_{i\in I_{\mathrm{dof}}^+}\langle \kappa_{\mathrm{dof}}\mathbf{u}_{\mathrm{dof}}, \mathbf{C}_i^{\mathrm{dof}}\rangle \bar{E}_i^{\mathrm{dof}} & \text{else,} \end{cases} \tag{13}$$

and: $I_{\mathrm{dof}}^+ = \{i, \langle \kappa_{\mathrm{dof}}\mathbf{u}_{\mathrm{dof}}, \mathbf{C}_i^{\mathrm{dof}}\rangle > 0\}$. The computation of $\mathbf{u}_{\mathrm{dof}}$ and $\bar{E}_j^{\mathrm{dof}}$ is described in the next sections. Eventually, the scheme reads as:

$$|\Omega_j|\frac{d}{dt}E_j + (1-\theta)\sum_{r\in\Omega_j}\left\langle \kappa_r\mathbf{u}_r, \mathbf{C}_j^r\right\rangle E_j^r + \theta\sum_{r+1/2\in\Omega_j}\left\langle \kappa_{r+1/2}\mathbf{u}_{r+1/2}, \mathbf{C}_j^{r+1/2}\right\rangle E_j^{r+1/2} = |\Omega_j|\mathcal{S}_j. \tag{14}$$

Proposition 3.1 (Conservation property)**.** *When the source term vanishes ($\mathcal{S} = 0$), the scheme (14)-(13) is conservative, that is to say, any solution $(E_j)_j$ to (14)-(13) satisfies:*

$$\frac{d}{dt}\left(\sum_{j\in\mathcal{T}} |\Omega_j| E_j\right) = 0.$$

Proof. The proof can be found in the Appendix of [BHL21]. □

4 First order fluxes : upwind scheme

We set:

$$\bar{E}_j^{\text{dof}} = E_j, \tag{15}$$

and $\mathbf{u}_{\text{dof}}$ is given by:

$$\mathbf{u}_r = \frac{1}{E_r}\beta_r^{-1} \sum_{i|r\in\Omega_i} E_i \mathbf{C}_i^r, \qquad E_r = \frac{1}{N_r}\sum_{i|r\in\Omega_i} E_i, \qquad \mathbf{u}_{r+1/2} = \frac{\mathbf{u}_r + \mathbf{u}_{r+1}}{2} \tag{16}$$

with:

$$\beta_r = \sum_{i|r\in\Omega_i} \mathbf{C}_i^r \otimes (\mathbf{x}_r - \mathbf{x}_i). \tag{17}$$

Under the assumptions of Section 2.2, the quantity $\mathbf{u}_{\text{dof}}$ defined in (16) is first order consistent with $-(\nabla E)_{\text{dof}}/E_{\text{dof}}$. Indeed, using a Taylor expansion, we have:

$$E(\mathbf{x}_i) = E(\mathbf{x}_r) + \langle \mathbf{x}_i - \mathbf{x}_r, \nabla E(\mathbf{x}_r)\rangle + O(h^2). \tag{18}$$

Multiplying (18) by $\mathbf{C}_i^r$, summing the result over the cells around any inner node r and using Proposition 2.3 leads to:

$$\sum_{i|r\in\Omega_i} E(\mathbf{x}_i)\mathbf{C}_i^r = E(\mathbf{x}_r) \underbrace{\sum_{i|r\in\Omega_i} \mathbf{C}_i^r}_{=\mathbf{0}} - \beta_r \nabla E(\mathbf{x}_r) + O(h^3), \tag{19}$$

where β_r is defined by (17). Using (11), we have:

$$\frac{1}{E(\mathbf{x}_r)}\beta_r^{-1}\left(\sum_{i|r\in\Omega_i} E(\mathbf{x}_i)\mathbf{C}_i^r\right) = \frac{-1}{E(\mathbf{x}_r)}(\nabla E)(\mathbf{x}_r) + O(h).$$

Moreover, $\mathbf{x}_i$ being the barycenter of the cell i, we have:

$$E(\mathbf{x}_i) = \frac{1}{|\Omega_i|}\int_{\Omega_i} E + O(h^2). \tag{20}$$

Using (16) (20), we deduce that $\mathbf{u}_r$ is first order consistent with $-(\nabla E)_r/E_r$. We easily deduce that $\mathbf{u}_{r+1/2}$ is first order consistent with $-(\nabla E)_{r+1/2}/E_{r+1/2}$.

Moreover, the following Lemma is useful in the proof of the positivity of the scheme (Proposition 4.2).

Lemma 4.1. *Let r be a given node. Under Assumptions (9) and (10), if all the $(E_i)_i$ are positive, then the nodal quantity $\mathbf{u}_r$ defined in (16) satisfies:*

$$\|\mathbf{u}_r\| \leq C_{4.1}\frac{1}{h},$$

Proof. Using (9) we have:

$$\left\| \frac{1}{E_r} \sum_{i|r\in\Omega_i} E_i \mathbf{C}_i^r \right\| = \left\| \frac{N_r}{\sum_{i|r\in\Omega_i} E_i} \sum_{i|r\in\Omega_i} E_i \mathbf{C}_i^r \right\| \leq C_1^3 h.$$

Using (11) gives the result. □

Proposition 4.2 (CFL condition)**.** *The explicit time discretisation of (14)-(13)-(15)-(16) preserves the positivity of the solution under the following condition:*

$$\Delta t \leq C_{4.2} \frac{h^2}{\kappa_2}.$$

Proof. We define:

$$R_j^+ = \{r \in \Omega_j, \quad \langle \kappa_r \mathbf{u}_r, \mathbf{C}_j^r \rangle > 0\}, \qquad R_j^- = \{r \in \Omega_j, \quad \langle \kappa_r \mathbf{u}_r, \mathbf{C}_j^r \rangle \leq 0\},$$

$$\tilde{R}_j^+ = \{r{+}1/2 \in \Omega_j, \quad \langle \kappa_{r+1/2} \mathbf{u}_{r+1/2}, \mathbf{C}_j^{r+1/2} \rangle > 0\}, \qquad \tilde{R}_j^- = \{r{+}1/2 \in \Omega_j, \quad \langle \kappa_{r+1/2} \mathbf{u}_{r+1/2}, \mathbf{C}_j^{r+1/2} \rangle \leq 0\}.$$

Equation (14) writes:

$$|\Omega_j| \frac{d}{dt} E_j + \left[(1-\theta) \sum_{r\in R_j^+} \left\langle \kappa_r \mathbf{u}_r, \mathbf{C}_j^r \right\rangle + \theta \sum_{r+1/2\in \tilde{R}_j^+} \left\langle \kappa_{r+1/2} \mathbf{u}_{r+1/2}, \mathbf{C}_j^{r+1/2} \right\rangle \right] E_j \tag{21}$$

$$+(1-\theta) \sum_{r\in R_j^-} \left\langle \kappa_r \mathbf{u}_r, \mathbf{C}_j^r \right\rangle E_j^r + \theta \sum_{r+1/2\in \tilde{R}_j^-} \left\langle \kappa_{r+1/2} \mathbf{u}_{r+1/2}, \mathbf{C}_j^{r+1/2} \right\rangle E_j^{r+1/2} = |\Omega_j| \mathcal{S}_j.$$

The explicit time discretisation of (21) reads as:

$$(E_j)^{n+1} = E_j \left(1 - \frac{\Delta t}{|\Omega_j|} \left[(1-\theta) \sum_{r\in R_j^+} \left\langle \kappa_r \mathbf{u}_r, \mathbf{C}_j^r \right\rangle + \theta \sum_{r+1/2\in \tilde{R}_j^+} \left\langle \kappa_{r+1/2} \mathbf{u}_{r+1/2}, \mathbf{C}_j^{r+1/2} \right\rangle \right] \right) \tag{22}$$

$$- \frac{\Delta t}{|\Omega_j|} \left[(1-\theta) \sum_{r\in R_j^-} \left\langle \kappa_r \mathbf{u}_r, \mathbf{C}_j^r \right\rangle E_j^r + \theta \sum_{r+1/2\in \tilde{R}_j^-} \left\langle \kappa_{r+1/2} \mathbf{u}_{r+1/2}, \mathbf{C}_j^{r+1/2} \right\rangle E_j^{r+1/2} \right] + \Delta t \mathcal{S}_j,$$

where we removed every upper script n in order to clarify the algebra. We have:

$$- \frac{\Delta t}{|\Omega_j|} \left[(1-\theta) \sum_{r\in R_j^-} \left\langle \kappa_r \mathbf{u}_r, \mathbf{C}_j^r \right\rangle E_j^r + \theta \sum_{r+1/2\in \tilde{R}_j^-} \left\langle \kappa_{r+1/2} \mathbf{u}_{r+1/2}, \mathbf{C}_j^{r+1/2} \right\rangle E_j^{r+1/2} \right] \geq 0. \tag{23}$$

Therefore, recalling that $\mathcal{S} \geq 0$, a natural stability condition writes:

$$\frac{\Delta t}{|\Omega_j|} \left[(1-\theta) \sum_{r\in R_j^+} \left\langle \kappa_r \mathbf{u}_r, \mathbf{C}_j^r \right\rangle + \theta \sum_{r+1/2\in \tilde{R}_j^+} \left\langle \kappa_{r+1/2} \mathbf{u}_{r+1/2}, \mathbf{C}_j^{r+1/2} \right\rangle \right] \leq 1.$$

Using Lemma 4.1, and Assumption (9), one has:

$$\frac{\Delta t}{|\Omega_j|} \left| (1-\theta) \sum_{r\in R_j^+} \left\langle \kappa_r \mathbf{u}_r, \mathbf{C}_j^r \right\rangle + \theta \sum_{r+1/2\in \tilde{R}_j^+} \left\langle \kappa_{r+1/2} \mathbf{u}_{r+1/2}, \mathbf{C}_j^{r+1/2} \right\rangle \right| \leq \underbrace{C_{4.1} C_1^3}_{:=C_{4.2}} \kappa_2 \frac{\Delta t}{h^2}. \tag{24}$$

Thus, if $\Delta t < h^2/(C_{4.2}\kappa_2)$ then $(E_j)^{n+1} > 0$, which gives the result.

□

Remark 1 (L^1 stability)**.** *The positivity of the numerical solution (Proposition 4.2) together with Proposition 3.1 imply that the explicit version of the scheme (14)-(13)-(15)-(16) is L^1 stable.*

5 Second order fluxes

Following some ideas of [BHL21], we propose a reconstruction procedure so as to make our scheme second order accurate in space. We only modify the computation of $\bar{E}_j^{\text{dof}}$:

$$\bar{E}_j^{\text{dof}} = \begin{cases} E_j - \langle \mathbf{v}_{\text{dof}}, \mathbf{x}_j - \mathbf{x}_{\text{dof}} \rangle & \text{if } |\langle \mathbf{v}_{\text{dof}}, \mathbf{x}_j - \mathbf{x}_{\text{dof}} \rangle| < E_j, \\ E_j & \text{else.} \end{cases} \tag{25}$$

The vector $\mathbf{v}_{\text{dof}}$ is an approximation of $\nabla E(\mathbf{x}_{\text{dof}})$ that is computed as follows:

$$\mathbf{v}_r = -E_r \mathbf{u}_r, \qquad \mathbf{v}_{r+1/2} = \frac{\mathbf{v}_r + \mathbf{v}_{r+1}}{2},$$

where $\mathbf{u}_r$ is given by (16). Note that if E_j is positive then $\bar{E}_j^{\text{dof}}$ is also positive. As it is shown in Section 7.2, it is not necessary to modify the computations of $\mathbf{u}_r$ and $\mathbf{u}_{r+1/2}$ in order to make the scheme second order consistent. Moreover, we can prove that this second order scheme is also positive under a parabolic CFL condition:

Proposition 5.1. *The explicit time discretisation of (14)-(13)-(16)-(25) preserves the positivity of the solution under the following condition:*

$$\Delta t \leq \frac{1}{2} C_{4.3} \frac{h^2}{\kappa_2}. \tag{26}$$

Proof. Using (25), we easily have:

$$\bar{E}_j^{\text{dof}} \leq 2E_j. \tag{27}$$

Therefore:

$$E_j^{n+1} \geq E_j \left(1 - 2\frac{\Delta t}{|\Omega_j|} \left[(1-\theta) \sum_{r \in R_j^+} \langle \kappa_r \mathbf{u}_r, \mathbf{C}_j^r \rangle + \theta \sum_{r+1/2 \in \tilde{R}_j^+} \left\langle \kappa_{r+1/2} \mathbf{u}_{r+1/2}, \mathbf{C}_j^{r+1/2} \right\rangle \right] \right).$$

Using Equation (24), we deduce that if $\Delta t < h^2/(2C_{4.2}\kappa_2)$ then $(E_j)^{n+1} > 0$, which gives the result.

□

6 Third order fluxes

In view of Theorem 2.2 we choose here $\theta = 2/3$ and we approximate the flux of Equation (12) by:

$$\int_{\partial\Omega_j} \langle \kappa \nabla E, \mathbf{n} \rangle \approx \frac{1}{3} \sum_{r \in \Omega_j} \langle \kappa_r \mathbf{u}_r, \mathbf{C}_j^r \rangle E_j^r + \frac{2}{3} \sum_{r+1/2 \in \Omega_j} \left\langle \kappa_{r+1/2} \mathbf{u}_{r+1/2}, \mathbf{C}_j^{r+1/2} \right\rangle E_j^{r+1/2},$$

We first compute a cell-wise polynomial approximation of E denoted by P_j:

$$P_j(\mathbf{x}) = E_j + \alpha_{j,E} \left[\langle (\nabla E)_j, \mathbf{x} - \mathbf{x}_j \rangle + \frac{1}{2} \langle (\nabla^2 E)_j \cdot (\mathbf{x} - \mathbf{x}_j), \mathbf{x} - \mathbf{x}_j \rangle \right] + K_j,$$

where $\alpha_{j,E}$ is a scalar limiter that ensures the positivity of P_j at any degree of freedom of the cell Ω_j. The gradient and the Hessian matrix are computed using a least-square procedure [BCHS20]. The constant K_j is chosen such that:

$$\frac{1}{|\Omega_j|}\int_{\Omega_j} P_j = E_j.$$

Then we set $\bar{E}_j^{\text{dof}} = P_j(\mathbf{x}_{\text{dof}})$. Moreover, noticing that $\nabla \ln|E| = (\nabla E)/E$ and recalling that $\mathbf{u}_{\text{dof}}$ has to be consistent with $(-\nabla(\ln E))_{\text{dof}}$, we compute it as:

$$\mathbf{u}_r = \frac{-1}{N_r}\sum_{i|r\in\Omega_i}\left[(\nabla\ln(|E|))_i + (\nabla^2\ln(|E|))_i\cdot(\mathbf{x}_r-\mathbf{x}_i)\right], \qquad \mathbf{u}_{r+1/2} = \frac{\mathbf{u}_r+\mathbf{u}_{r+1}}{2}. \tag{28}$$

The gradient $(\nabla\ln(|E|))_i$ and Hessian matrix $(\nabla^2\ln(|E|))_i$ are computed with the same least-square method as in [BCHS20]. As it is shown in Section 7.3, it is sufficient to compute a second order approximation of $\nabla\ln|E|$ in order to make the scheme third order consistent.

The quantity $\mathbf{u}_{\text{dof}}$ computed with (28) is second order consistent with $-\nabla\ln|E|(\mathbf{x}_{\text{dof}})$. Indeed, using a Taylor expansion, we have:

$$\nabla\ln|E|(\mathbf{x}_{\text{dof}}) = \nabla\ln|E|(\mathbf{x}_i) + (\nabla^2\ln(|E|))(\mathbf{x}_i)\cdot(\mathbf{x}_r-\mathbf{x}_i) + O(h^2).$$

Therefore $\mathbf{u}_r$ computed with (28) is second order consistent with $-\nabla\ln|E|(\mathbf{x}_r)$. Moreover, $\mathbf{x}_{r+1/2}$ being the midpoint of the edge $[\mathbf{x}_r,\mathbf{x}_{r+1}]$, the quantity $\mathbf{u}_{r+1/2}$ is second order consistent with $-\nabla\ln|E|(\mathbf{x}_{r+1/2})$.

7 Numerical results

In this section, we provide some numerical examples that illustrate the good properties of our scheme. In Section 7.1 we present the test cases. The results with the second order scheme are presented in Section 7.2 and the results with the third order scheme are shown in Section 7.3.

7.1 Presentation of the test cases

We use an explicit time discretisation. The time step is given by $\Delta t = C_{CFL}h^2$ where the constant C_{CFL} depends on the test case. For the test cases of Sections 7.1.2 and 7.1.3, we define the analytical solution E and compute the source term $\mathcal{S}$ such that E satisfies Equation (1). We use cartesian meshes, random meshes (see Figure 2), Kershaw type meshes (see Figure 3). We denote by N_x the number of cells in the x direction and N_y the number of cells in the y direction.
Moreover, it is well known that the purely nodal scheme ($\theta = 0$ in (14)) may exhibit some *cross-stencil* propagation on cartesian meshes. This issue is corrected using the composite scheme ($\theta > 0$ in (14)). We do not give here any illustration of this property, examples can be found in [BHL21].
The space step is $h = \Delta x = 1/N_x = \Delta y = 1/N_y$. The final time is denoted by t_f. Periodic boundary conditions are imposed.

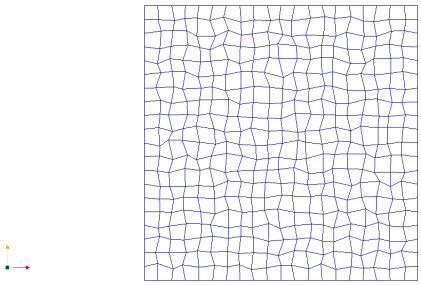

Figure 2: Random mesh of size 20×20.

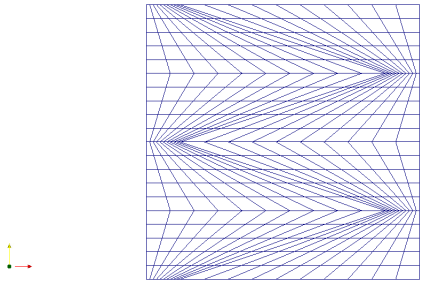

Figure 3: Kershaw type mesh of size 20×20

7.1.1 Fundamental solution of the diffusion equation

This test case is borrowed from [BHL21]. We set $\kappa = I_2/3$ and $\mathcal{S} = 0$, thus (1) reads as:

$$\partial_t E - \frac{1}{3}\Delta E = 0. \tag{29}$$

The exact solution of (29) satisfying $E(t=0) = \delta_{\mathbf{x_0}}$ for a given $\mathbf{x_0}$ is:

$$E(t, \mathbf{x}) = \frac{3}{4\pi t} \exp\left(-3\frac{\|\mathbf{x} - \mathbf{x_0}\|^2}{4t}\right). \tag{30}$$

The initial data is $E(t = t_0)$ and the exact solution is $E(t = t_0 + t_f)$ with $t_0 = 0.01$ and where t_f is the final time. We choose $\mathbf{x_0} = (0.5, 0.5)$. The computational domain is $\Omega = [0, 1]^2$. The boundary conditions do not affect the result since the solution is almost 0 on the boundary.

7.1.2 $1D$ test case

For $\mathbf{x} = (x, y)$, the diffusion coefficient is given by:

$$\kappa(\mathbf{x}) = \frac{1}{\pi^2} \exp\left(\sin(2\pi x) - 1\right), \qquad E(x, t) = \exp\left(t - \sin(2\pi x)\right). \tag{31}$$

Thus (1) becomes:

$$\partial_t E - \frac{1}{\pi^2}\partial_x \left[\exp\left(\sin(2\pi x) - 1\right)\partial_x E\right] = \mathcal{S},$$

with:

$$\mathcal{S}(t, \mathbf{x}) = \mathcal{S}(t, x) = e^t \left[\exp\left(-\sin(2\pi x)\right) - e^{-1}\sin(2\pi x)\right].$$

Periodic boundary conditions are imposed. The computational domain is $\Omega = [0, 1]^2$. The initial condition is given by $E(t = 0)$ in (31).

7.1.3 Anisotropic $2D$ test case

This test case is inspired from [LP20] and [CCP13]. The computational domain is $\Omega = [0, 2]^2$. The solution reads as:

$$E(t, \mathbf{x}) = \left[2 + \sin(\pi x)\sin(\pi y)\right] e^{\lambda t}, \qquad \lambda = 11. \tag{32}$$

The diffusion coefficient is given by:

$$\kappa(x, y) = \frac{1}{x^2 + y^2}\begin{pmatrix} y^2 + \alpha x^2 & -(1-\alpha)xy \\ -(1-\alpha)xy & x^2 + \alpha y^2 \end{pmatrix}, \qquad \alpha = 10^{-6}. \tag{33}$$

Its eigenvalues are 1 and α.

7.2 Results with the second order scheme

In this section, we present some convergence analysis for the test cases of Section 7.1 using the scheme of Section 5. The final time is $t_f = 0.003$. The initial condition and the error are computed as:

$$E_j^0 = E^{\text{exact}}(0, \mathbf{x}_j), \qquad e = \sum_{j \in \mathcal{T}} |\Omega_j| \left| E^{\text{exact}}(t_f, \mathbf{x}_j) - E_j \right|,$$

Figure 4 shows the errors for the test case of Section 7.1.1 on different meshes. Figure 5 shows the errors for the test case of Section 7.1.2 on different meshes. Figure 6 shows the errors for the test case of Section 7.1.3 on different meshes. The constant C_{CFL} is smaller on the very deformed meshes (Kershaw and non-convex type meshes) due to stability reasons. We see that the scheme is second order convergent on every type of meshes.

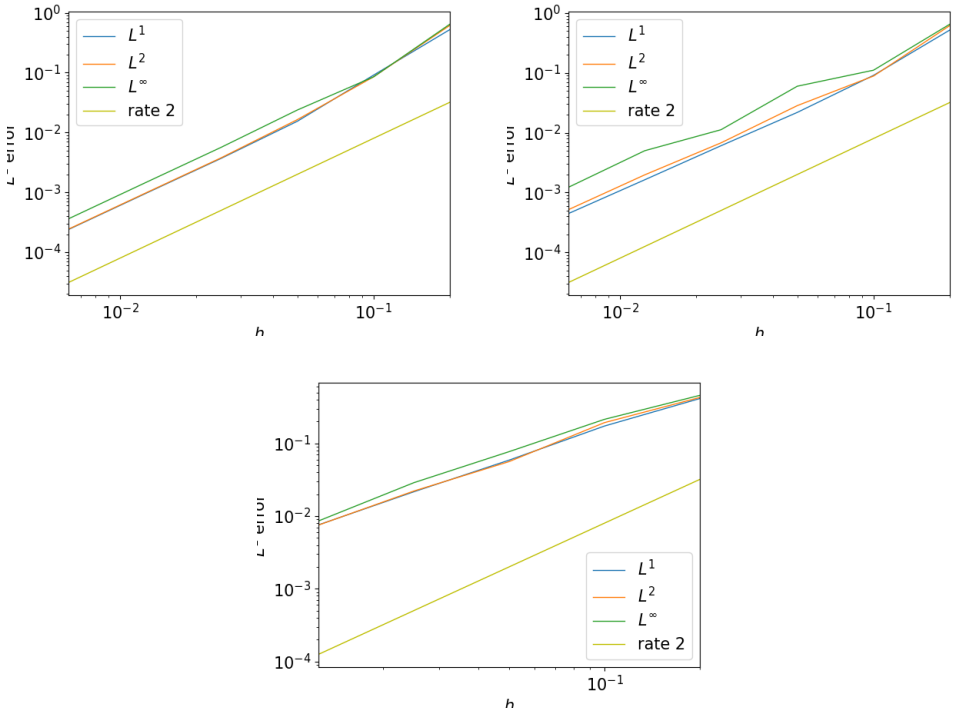

Figure 4: Errors at $t = 0.003$ and $\theta = 2/3$ and initial condition given in (30) on cartesian and $C_{CFL} = 0.5$(up left), on random meshes (see Figure 2) and $C_{CFL} = 0.5$ (up right), and on Kershaw type mesh (see Figure 3) and $C_{CFL} = 0.01$ (down).

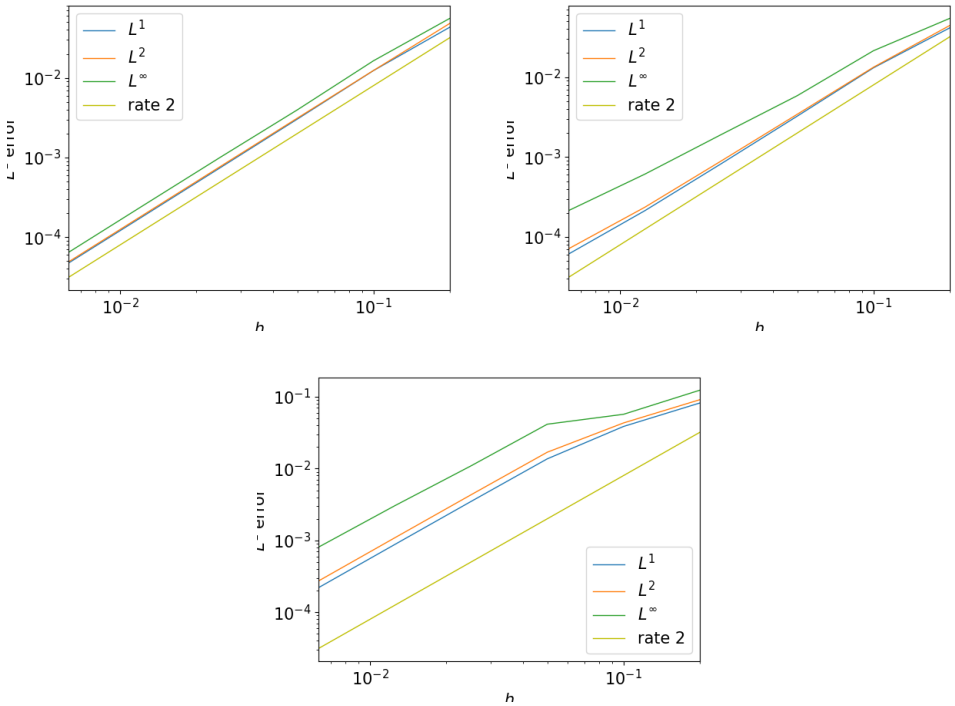

Figure 5: Errors at $t = 0.003$ and $\theta = 2/3$ and initial condition given in (31) on cartesian meshes $C_{CFL} = 0.5$ (up left), on random meshes and $C_{CFL} = 0.5$ (up right) and on Kershaw type meshes and $C_{CFL} = 0.1$ (down).

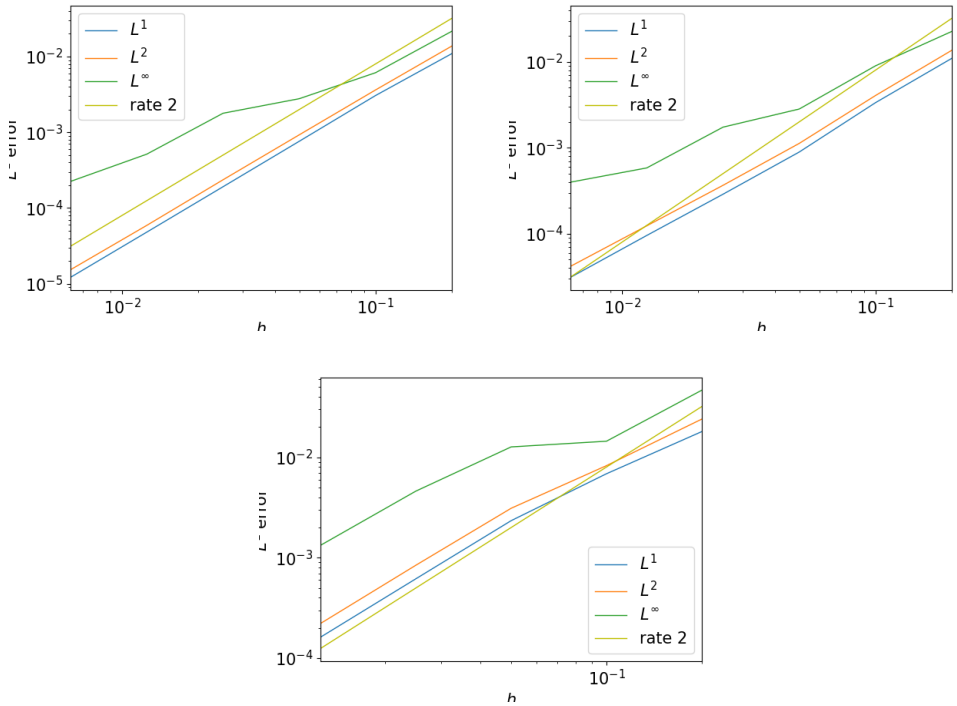

Figure 6: Errors at $t = 0.003$ and $\theta = 2/3$ and initial condition given in (32) on cartesian meshes and $C_{CFL} = 0.5$ (up left), on random meshes and $C_{CFL} = 0.1$ (up right), on Kershaw type meshes and $C_{CFL} = 0.005$ (down).

7.3 Results with the third order scheme

In this section, we present some convergence analysis for the test cases of Section 7.1 using the scheme of Section 5. We use a third order Runge-Kutta scheme to discretise the time derivative. The final time is $t_f = 0.001$. The initial data is given by:

$$E_j^0 = \frac{1}{|\Omega_j|} \int_{\Omega_j} E^{\text{exact}}(0, \mathbf{x}) d\mathbf{x},$$

and the error is computed as follows:

$$e = \sum_{j \in \mathcal{T}} \int_{\Omega_j} \left| E^{\text{exact}}(t_f, \mathbf{x}) - P_j(\mathbf{x}) \right| d\mathbf{x},$$

Figure 7 shows the errors for the test case of Section 7.1.1 on different meshes. Figure 8 shows the errors for the test case of Section 7.1.2 on different meshes. Figure 9 shows the errors for the test case of Section 7.1.3 on different meshes. We see that the scheme is third order convergent on every type of meshes.

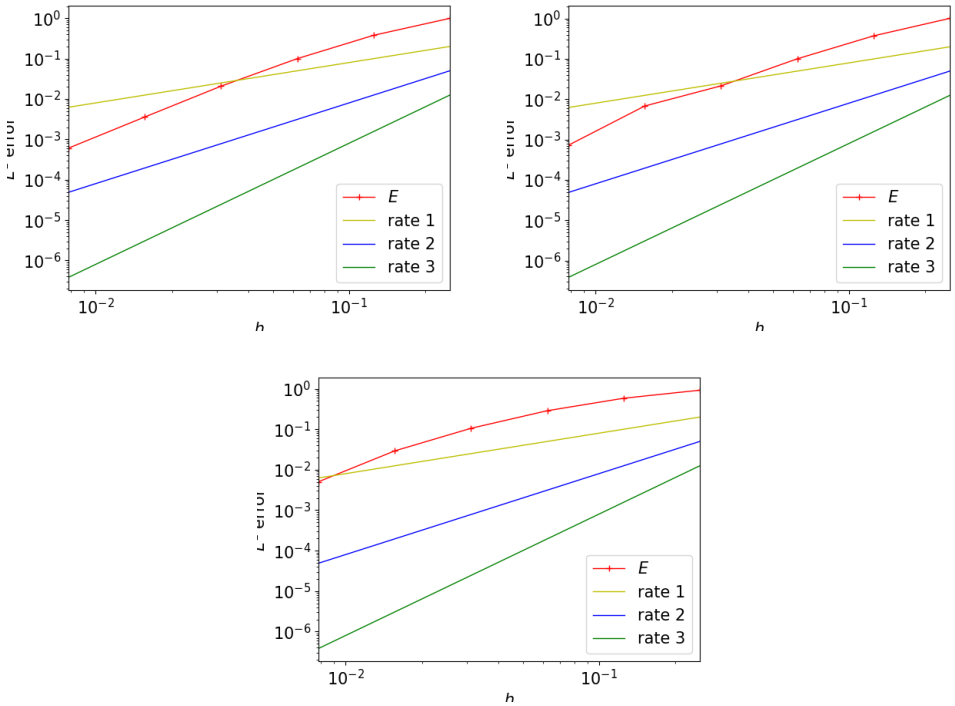

Figure 7: L^1 error at $t = 0.001$ and initial condition given in (30) on cartesian meshes (up left), on random meshes (up right), on Kershaw type meshes (down) and $C_{CFL} = 0.4$.

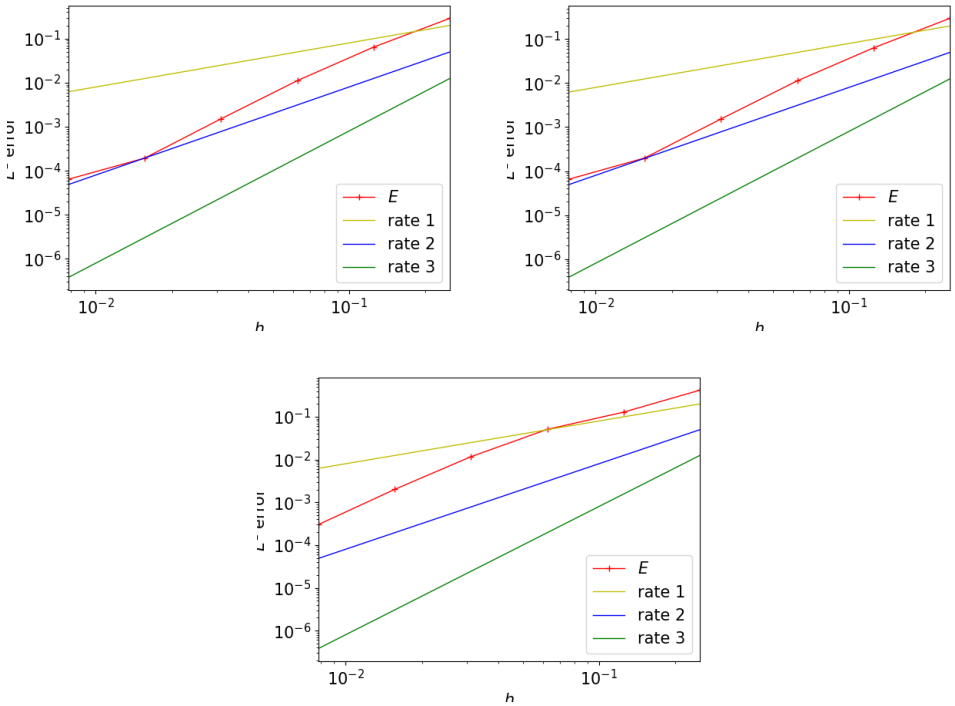

Figure 8: L^1 error at $t = 0.001$ and initial condition given in (31) on cartesian meshes (up left), on random meshes (up right), on Kershaw type meshes (down) and $C_{CFL} = 0.4$.

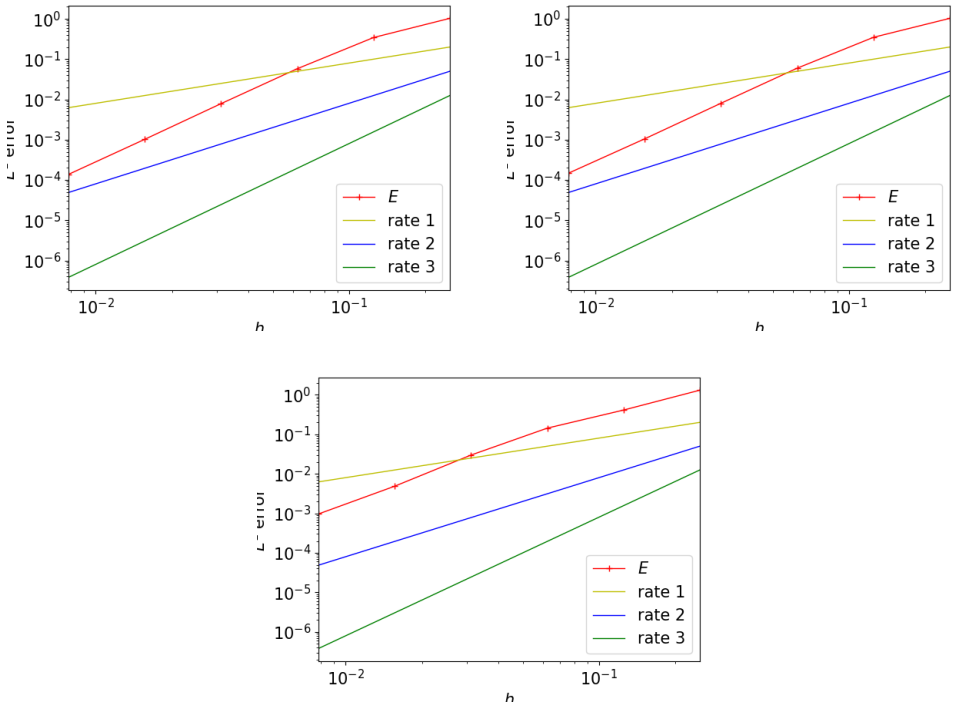

Figure 9: L^1 error at $t = 0.001$ and initial condition given in (32) on cartesian meshes and $C_{CFL} = 0.02$ (up left), on random meshes and $C_{CFL} = 0.02$ (up right), on Kershaw type meshes and $C_{CFL} = 0.005$ (down).

8 Appendix

8.1 Periodic boundary conditions

The boundary conditions are imposed using the method described in [BHL21]. In the case of periodic boundary conditions, we add some *ghost* cells on the outside of the mesh so as to make it periodic. We then define the unknown E on these new cells so as to make it periodic and we use this new geometric data to compute the matrix β_r on the boundary of the domain.

8.2 Proof of Theorem 2.1

Let $j \in \mathcal{T}$, we show the following equality: for any $\boldsymbol{\xi} \in \mathbb{R}^2$ and any $\theta \in [0,1]$,

$$\int_{\partial\Omega_j} \langle \boldsymbol{\xi}, \mathbf{x} \rangle \mathbf{n} d\mathbf{x} = (1-\theta) \sum_{r \in \Omega_j} \langle \boldsymbol{\xi}, \mathbf{x}_r \rangle \mathbf{C}_j^r + \theta \sum_{r+1/2 \in \Omega_j} \langle \boldsymbol{\xi}, \mathbf{x}_{r+1/2} \rangle \mathbf{C}_j^{r+1/2}. \tag{34}$$

On the one hand, we have

$$\int_{\partial\Omega_j} \langle \boldsymbol{\xi}, \mathbf{x} \rangle \mathbf{n} d\mathbf{x} = \sum_{r+1/2 \in \Omega_j} \left(\int_{x_r}^{x_{r+1}} \langle \boldsymbol{\xi}, \mathbf{x} \rangle \mathbf{n} d\mathbf{x} \right).$$

On each edge, the outward unit normal vector $\mathbf{n}$ is constant and it is given by $\mathbf{n}_j^{r+1/2} = \mathbf{C}_j^{r+1/2} / \|\mathbf{C}_j^{r+1/2}\|$. Therefore we have:

$$\sum_{r+1/2 \in \Omega_j} \left(\int_{x_r}^{x_{r+1}} \langle \boldsymbol{\xi}, \mathbf{x} \rangle \mathbf{n} d\mathbf{x} \right) = \sum_{r+1/2 \in \Omega_j} \left\langle \boldsymbol{\xi}, \underbrace{\int_{\mathbf{x}_r}^{\mathbf{x}_{r+1}} \mathbf{x} d\mathbf{x}}_{= \|\mathbf{x}_{r+1} - \mathbf{x}_r\| \mathbf{x}_{r+1/2}} \right\rangle \mathbf{n}_j^{r+1/2} = \sum_{r+1/2 \in \Omega_j} \langle \boldsymbol{\xi}, \mathbf{x}_{r+1/2} \rangle \mathbf{C}_j^{r+1/2}.$$

Moreover, we have:

$$\sum_{r+1/2\in\Omega_j} \langle \boldsymbol{\xi}, \mathbf{x}_{r+1/2}\rangle \, \mathbf{C}_j^{r+1/2} = \sum_{r\in\Omega_j} \langle \boldsymbol{\xi}, \mathbf{x}_r\rangle \, \mathbf{C}_j^{r}. \tag{35}$$

Indeed, using (6) leads to:

$$\begin{aligned}\sum_{r\in\Omega_j} \langle \boldsymbol{\xi}, \mathbf{x}_r\rangle \, \mathbf{C}_j^{r} &= \frac{1}{2}\sum_{r\in\Omega_j} \langle \boldsymbol{\xi}, \mathbf{x}_r\rangle \, \mathbf{C}_j^{r-1/2} + \frac{1}{2}\sum_{r\in\Omega_j} \langle \boldsymbol{\xi}, \mathbf{x}_r\rangle \, \mathbf{C}_j^{r+1/2} \\ &= \frac{1}{2}\sum_{r+1/2\in\Omega_j} \langle \boldsymbol{\xi}, \mathbf{x}_{r+1}\rangle \, \mathbf{C}_j^{r+1/2} + \frac{1}{2}\sum_{r+1/2\in\Omega_j} \langle \boldsymbol{\xi}, \mathbf{x}_r\rangle \, \mathbf{C}_j^{r+1/2},\end{aligned}$$

which gives (35). This proves (34) and gives the result (7).

8.3 Proof of Theorem 2.2

We prove the following equality, for any matrix $A \in \mathbb{R}^{2\times 2}$:

$$\int_{\partial\Omega_j} \langle \mathbf{x}, A\mathbf{x}\rangle \mathbf{n} d\mathbf{x} = \frac{1}{3}\sum_{r\in\Omega_j} \langle \mathbf{x}_r, A\mathbf{x}_r\rangle \mathbf{C}_j^r + \frac{2}{3}\sum_{r+1/2\in\Omega_j} \langle \mathbf{x}_{r+1/2}, A\mathbf{x}_{r+1/2}\rangle \mathbf{C}_j^{r+1/2}. \tag{36}$$

Using (6), one has:

$$\sum_{r\in\Omega_j} \langle \mathbf{x}_r, A\mathbf{x}_r\rangle \mathbf{C}_j^r = \frac{1}{2}\sum_{r+1/2\in\Omega_j} (\langle \mathbf{x}_r, A\mathbf{x}_r\rangle + \langle \mathbf{x}_{r+1}, A\mathbf{x}_{r+1}\rangle) \mathbf{C}_j^{r+1/2}.$$

This implies:

$$\begin{aligned}&\frac{1}{3}\sum_{r\in\Omega_j} \langle \mathbf{x}_r, A\mathbf{x}_r\rangle \mathbf{C}_j^r + \frac{2}{3}\sum_{r+1/2\in\Omega_j} \langle \mathbf{x}_{r+1/2}, A\mathbf{x}_{r+1/2}\rangle \mathbf{C}_j^{r+1/2} \\ = &\sum_{r+1/2\in\Omega_j} \left[\frac{2}{3}\langle \mathbf{x}_{r+1/2}, A\mathbf{x}_{r+1/2}\rangle + \frac{1}{6}\left(\langle \mathbf{x}_r, A\mathbf{x}_r\rangle + \langle \mathbf{x}_{r+1}, A\mathbf{x}_{r+1}\rangle\right)\right] \mathbf{C}_j^{r+1/2}.\end{aligned}$$

Moreover we have:

$$\frac{2}{3}\langle \mathbf{x}_{r+1/2}, A\mathbf{x}_{r+1/2}\rangle + \frac{1}{6}\left(\langle \mathbf{x}_r, A\mathbf{x}_r\rangle + \langle \mathbf{x}_{r+1}, A\mathbf{x}_{r+1}\rangle\right) \tag{37}$$

$$= \frac{1}{6}\left[\langle \mathbf{x}_r, A\mathbf{x}_{r+1}\rangle + \langle \mathbf{x}_{r+1}, A\mathbf{x}_r\rangle + 2\langle \mathbf{x}_r, A\mathbf{x}_r\rangle + 2\langle \mathbf{x}_{r+1}, A\mathbf{x}_{r+1}\rangle\right]. \tag{38}$$

Eventually, we note that:

$$\int_{\partial\Omega_j} \langle \mathbf{x}, A\mathbf{x}\rangle \mathbf{n} d\mathbf{x} = \sum_{r+1/2\in\Omega_j} \left(\int_0^1 \langle \lambda\mathbf{x}_r + (1-\lambda)\mathbf{x}_{r+1}, A(\lambda\mathbf{x}_r + (1-\lambda)\mathbf{x}_{r+1})\rangle d\lambda\right) \mathbf{C}_j^{r+1/2}, \tag{39}$$

and:

$$\int_0^1 \langle \lambda\mathbf{x}_r + (1-\lambda)\mathbf{x}_{r+1}, A(\lambda\mathbf{x}_r + (1-\lambda)\mathbf{x}_{r+1})\rangle \tag{40}$$

$$= \frac{1}{6}\left[\langle \mathbf{x}_r, A\mathbf{x}_{r+1}\rangle + \langle \mathbf{x}_{r+1}, A\mathbf{x}_r\rangle + 2\langle \mathbf{x}_r, A\mathbf{x}_r\rangle + 2\langle \mathbf{x}_{r+1}, A\mathbf{x}_{r+1}\rangle\right]. \tag{41}$$

Collecting (37), (39) and (40), we find (36) and the desired result.

References

[AEK+07] I. Aavatsmark, G.T. Eigestad, R.A. Klausen, M.F. Wheeler, and I. Yotov. Convergence of a symmetric MPFA method on quadrilateral grids. *Comput. Geosci.*, 11(4):333–345, 2007.

[AN21] Ashwani Assam and Ganesh Natarajan. A novel least squares finite volume scheme for discontinuous diffusion on unstructured meshes. *Comput. Math. Appl.*, 96:120–130, 2021.

[AWY97] Todd Arbogast, Mary F. Wheeler, and Ivan Yotov. Mixed finite elements for elliptic problems with tensor coefficients as cell-centered finite differences. *SIAM J. Numer. Anal.*, 34(2):828–852, 1997.

[BBL09] Franco Brezzi, Annalisa Buffa, and Konstantin Lipnikov. Mimetic finite differences for elliptic problems. *ESAIM, Math. Model. Numer. Anal.*, 43(2):277–295, 2009.

[BCHS20] Aude Bernard-Champmartin, Philippe Hoch, and Nicolas Seguin. Stabilité locale et montée en ordre pour la reconstruction de quantités volumes finis sur maillages coniques non-structurés en dimension 2. preprint, `https://hal.archives-ouvertes.fr/hal-02497832`, March 2020.

[BHL21] Xavier Blanc, Philippe Hoch, and Clément Lasuen. An asymptotic preserving scheme for the M1 model on conical meshes. working paper or preprint, 2021.

[BL16] Xavier Blanc and Emmanuel Labourasse. A positive scheme for diffusion problems on deformed meshes. *ZAMM - Journal of Applied Mathematics and Mechanics / Zeitschrift für Angewandte Mathematik und Mechanik*, 96(6):660–680, 2016.

[BM05] Enrico Bertolazzi and Gianmarco Manzini. A second-order maximum principle preserving finite volume method for steady convection-diffusion problems. *SIAM J. Numer. Anal.*, 43(5):2172–2199, 2005.

[BM07] Jérôme Breil and Pierre-Henri Maire. A cell-centered diffusion scheme on two-dimensional unstructured meshes. *J. Comput. Phys.*, 224(2):785–823, 2007.

[CCP13] Clément Cancès, Mathieu Cathala, and Christophe Potier. Monotone corrections for generic cell-centered finite volume approximations of anisotropic diffusion equations. *Numerische Mathematik*, 125, 11 2013.

[CVV99] Yves Coudière, Jean-Paul Vila, and Philippe Villedieu. Convergence rate of a finite volume scheme for a two-dimensional convection-diffusion problem. *M2AN Math. Model. Numer. Anal.*, 33(3):493–516, 1999.

[DF99] Bruno Dubroca and Jean-Luc Feugeas. Étude théorique et numérique d'une hiérarchie de modèles aux moments pour le transfert radiatif. *C. R. Acad. Sci. Paris Sér. I Math.*, 329(10):915–920, 1999.

[Eym10] Eymard, R. and Gallouët, T. and Herbin, R. Discretization of heterogeneous and anisotropic diffusion problems on general nonconforming meshes SUSHI: A scheme using stabilization and hybrid interfaces. *IMA J. Numer. Anal.*, 30(4):1009–1043, 2010.

[FBD11] Emmanuel Franck, Christophe Buet, and Bruno Després. Asymptotic preserving finite volumes discretization for non-linear moment model on unstructured meshes. In *Finite volumes for complex applications VI. Problems & perspectives. Volume 1, 2*, volume 4 of *Springer Proc. Math.*, pages 467–474. Springer, Heidelberg, 2011.

[Fra12] Emmanuel Franck. *Construction et analyse numérique de schema asymptotic preserving sur maillages non structurés. Application au transport linéaire et aux systèmes de Friedrichs.* PhD thesis, Université Pierre et Marie Curie - Paris VI, 2012.

[Her98] F. Hermeline. A finite volume method for second-order elliptic equations. (Une méthode de volumes finis pour les équations elliptiques du second ordre.). *C. R. Acad. Sci. Paris, Ser. I*, 1998.

[Her00] F. Hermeline. A finite volume method for the approximation of diffusion operators on distorted meshes. *J. Comput. Phys.*, 160(2):481–499, 2000.

[Her03] F. Hermeline. Approximation of diffusion operators with discontinuous tensor coefficients on distorted meshes. *Comput. Methods Appl. Mech. Eng.*, 192(16-18):1939–1959, 2003.

[Her07] F. Hermeline. Approximation of 2D and 3D diffusion operators with variable full tensor coefficients on arbitrary meshes. *Comput. Methods Appl. Mech. Eng.*, 196(21-24):2497–2526, 2007.

[Hoc22] Philippe Hoch. Nodal extension of Approximate Riemann Solvers and nonlinear high order reconstruction for finite volume method on unstructured polygonal and conical meshes: the homogeneous case. working paper or preprint, February 2022.

[Ker81] David S. Kershaw. Differencing of the diffusion equation in Lagrangian hydrodynamic codes. *J. Comput. Phys.*, 39:375–395, 1981.

[LMS14] Konstantin Lipnikov, Gianmarco Manzini, and Mikhail Shashkov. Mimetic finite difference method. *Journal of Computational Physics*, 257, Part B(0):1163 – 1227, 2014. Physics-compatible numerical methods.

[LP09] Christophe Le Potier. A nonlinear finite volume scheme satisfying maximum and minimum principles for diffusion operators. *Int. J. Finite Vol.*, 6(2):20, 2009.

[LP20] Christophe Le Potier. A second order in space combination of methods verifying a maximum principle for the discretization of diffusion operators. *C. R. Math. Acad. Sci. Paris*, 358(1):89–96, 2020.

[NSL22] Cunyun Nie, Shi Shu, and Menghuan Liu. A novel monotone finite volume element scheme for diffusion equations. *J. Comput. Appl. Math.*, 414:Paper No. 114458, 20, 2022.

[Per81] G. J. Pert. Physical constraints in numerical calculations of diffusion. *J. Comput. Phys.*, 42(1):20–52, 1981.

[RB17] Aníbal Rodríguez-Bernal. The heat equaton with general periodic boundary conditions. *Potential Anal.*, 46(2):295–321, 2017.

[RT83] P.-A. Raviart and J.-M. Thomas. *Introduction à l'analyse numérique des équations aux dérivées partielles*. Collection Mathématiques Appliquées pour la Maîtrise. [Collection of Applied Mathematics for the Master's Degree]. Masson, Paris, 1983.

[SY16] Zhiqiang Sheng and Guangwei Yuan. A new nonlinear finite volume scheme preserving positivity for diffusion equations. *J. Comput. Phys.*, 315:182–193, 2016.

[SYY09] Zhiqiang Sheng, Jingyan Yue, and Guangwei Yuan. Monotone finite volume schemes of nonequilibrium radiation diffusion equations on distorted meshes. *SIAM J. Sci. Comput.*, 31(4):2915–2934, 2009.

[WPL+22] Xiaoxin Wu, Kejia Pan, Jin Li, Yunlong Yu, Guangwei Yuan, and Zhengyong Ren. A robust, interpolation-free and monotone finite volume scheme for diffusion equations on arbitrary quadrilateral meshes. *Internat. J. Numer. Methods Engrg.*, 123(16):3631–3657, 2022.

[YSGN22] Di Yang, Meihua Sheng, Zhiming Gao, and Guoxi Ni. The VEM-based positivity-preserving conservative scheme for radiation diffusion problems on generalized polyhedral meshes. *Comput. & Fluids*, 239:Paper No. 105356, 20, 2022.